

**Materials Synthesis**

# An Unexpected Cubic Symmetry in Group IV Alloys Prepared Using Pressure and Temperature

George Serghiou,\* Hans Josef Reichmann, Nicholas Odling, Kristina Spektor, Anna Pakhomova, Wilson A. Crichton, and Zuzana Konôpková

**Abstract:** The cubic diamond ( $Fd\bar{3}m$ ) group IVA element Si has been the material driver of the electronics industry since its inception. We report synthesis of a new cubic ( $Im\bar{3}m$ ) group IVA material, a GeSn solid solution, upon heating Ge and Sn at pressures from 13 to 28 GPa using double-sided diamond anvil laser-heating and large volume press methods. Both methods were coupled with in situ angle dispersive X-ray diffraction characterization. The new material substantially enriches the seminal group IVA alloy materials landscape by introducing an eightfold coordinated cubic symmetry, which markedly expands on the conventional tetrahedrally coordinated cubic one. This cubic solid solution is formed, despite Ge never adopting the  $Im\bar{3}m$  symmetry, melting inhibiting subsequent  $Im\bar{3}m$  formation and reactant Ge and Sn having unlike crystal structures and atomic radii at all these pressures. This is hence achieved without adherence to conventional formation criteria and routes to synthesis. This advance creates fertile avenues for new materials development.

## Introduction

Despite the overwhelming importance of cubic diamond Si in electronic applications, its indirect band-gap and fixed lattice constant make it considerably less effective for optoelectronic applications.<sup>[1]</sup> While solid solution with isostructural Ge facilitates tunability of both lattice constant and band-gap, the SiGe band-gaps remain indirect.<sup>[2,3]</sup> Conversely, alloying Ge with Sn can provide tunability and direct band-gap formation making this one of the most actively investigated systems for optoelectronic applications.<sup>[4–7]</sup> These investigations are mostly confined to thin films because Ge and Sn are immiscible in the bulk at ambient pressure.<sup>[8,9]</sup> Change in miscibility and bulk synthesis can however be


achieved using high pressure and temperature to access regions of the phase diagram where Ge and Sn become similar enough.<sup>[10]</sup> Between ambient pressure and 10 GPa Ge adopts a cubic structure with  $Fd\bar{3}m$  symmetry whereas Sn adopts a tetragonal structure with  $I4_1/amd$  symmetry ( $\beta$ -Sn). At 10 GPa cubic Ge also transforms to the tetragonal structure with  $I4_1/amd$  symmetry ( $\beta$ -Ge). Sn on other hand, transforms above 10 GPa to another tetragonal structure with  $I4/mmm$  symmetry (t-Sn).<sup>[11]</sup>  $\beta$ - and t- throughout always designate the  $I4_1/amd$  and  $I4/mmm$  space groups, respectively. The only pressure where Ge and Sn can be similar enough according to the Hume-Rothery criteria,<sup>[12]</sup> is at 10 GPa. In particular, based on the consideration that at 10 GPa Ge and Sn could uniquely adopt the same tetragonal crystal structure with  $I4_1/amd$  symmetry and have atomic radii ratios below the Hume-Rothery 15 % tolerance threshold, we heated Ge and Sn at this pressure and indeed recovered a bulk GeSn solid solution with  $P4_32_12$  symmetry.<sup>[10,13]</sup> However, several further heating experiments above this a priori unique pressure, at between 11–24 GPa also led to recovery of bulk GeSn solid solutions, frequently nanocrystalline<sup>[14]</sup> with the cubic diamond structure, containing up to 30 at % Sn. This surprising result indicated that reaction between Ge and Sn was occurring with facility in an extended pressure regime, where it was considered unfavourable.


## Results

To investigate this high pressure region for potential existence of a hidden alloy structure, we performed numerous experiments using both laser-heated diamond anvil cell and scale-up multianvil methods, both of which were coupled with

[\*] Dr. G. Serghiou  
 School of Engineering, University of Edinburgh, Kings Buildings  
 Robert Stevenson Road, Edinburgh EH9 3FB, Scotland (UK)  
 E-mail: george.serghiou@ed.ac.uk  
 Dr. H. J. Reichmann  
 Deutsches GeoforschungsZentrum, GFZ  
 Telegrafenberg, 14473 Potsdam (Germany)  
 Dr. N. Odling  
 School of Geosciences, University of Edinburgh, Kings Buildings  
 West Mains Road, Edinburgh EH9 3JW, Scotland (UK)  
 Dr. K. Spektor, Dr. W. A. Crichton  
 The European Synchrotron, ESRF  
 71 avenue des Martyrs, 38000 Grenoble (France)

Dr. A. Pakhomova, Dr. Z. Konôpková  
 Deutsches Elektronen-Synchrotron, DESY  
 22607 Hamburg (Germany)  
 Dr. Z. Konôpková  
 European XFEL GmbH  
 Holzkoppel 4, 22869 Schenefeld (Germany)

 Supporting information and the ORCID identification number(s) for the author(s) of this article can be found under <https://doi.org/10.1002/anie.202016179>.

 © 2021 The Authors. Angewandte Chemie International Edition published by Wiley-VCH GmbH. This is an open access article under the terms of the Creative Commons Attribution Non-Commercial License, which permits use, distribution and reproduction in any medium, provided the original work is properly cited and is not used for commercial purposes.

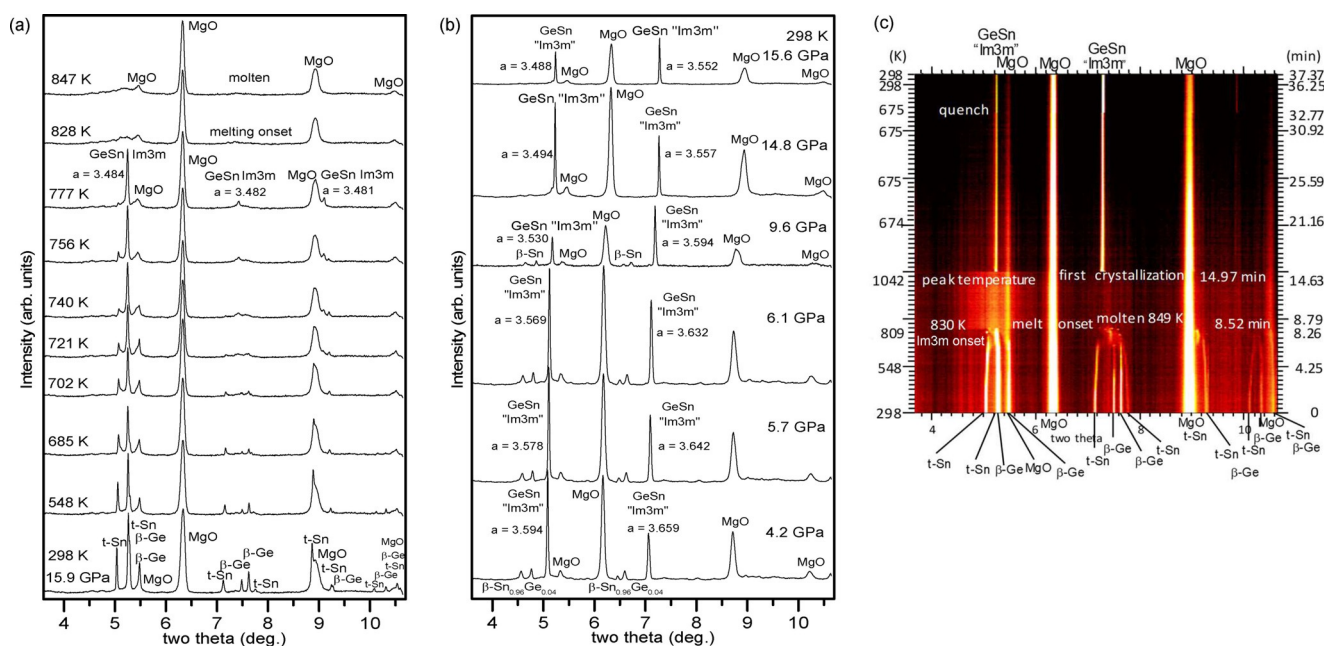


**Figure 1.** a) Angle-dispersive X-ray diffraction patterns upon heating and melting of a  $\beta$ -Ge and t-Sn mixture at 15.9 GPa in a multi-anvil device and formation of a bcc structure with *Im* $\bar{3}$ *m* symmetry [ $a = 3.481(1) \text{ \AA}$ ] at 777 K (Figure S6, Le Bail fitting in the supporting information)<sup>[15]</sup> before melting. b) Upon re-crystallization a structure with a nominal "*Im* $\bar{3}$ *m*" symmetry exhibits significant anisotropy and diffraction intensity variation. Indexing of this structure is consistent with the *I4/mmm* symmetry with a  $c/a = 0.97$  [ $a = 3.552(1) \text{ \AA}$ ,  $c = 3.430(1) \text{ \AA}$ ] (top pattern) (Figure S7, Le Bail fitting in the supporting information)<sup>[15]</sup> which is not far from cubic. This phase, with this  $c/a$  ratio, is stable down to 4.2 GPa with exsolution of  $\beta$ -Sn beginning below 10 GPa (Figure S8–12, Le Bail fitting in the supporting information).<sup>[15]</sup> c) Time-temperature-intensity-two-theta plot at 15.9 GPa through melting and upon annealing on re-solidification and then temperature quenching. The left and right horizontal bars are not scales, but references to correlate times on the right vertical axis with their corresponding temperatures on the left vertical axis.

requisite in situ angle dispersive monochromatic synchrotron X-ray diffraction.<sup>[15]</sup> We present examples from both types of experiments. The first example is from one of our multi-anvil studies where a 60:40 at %  $\beta$ -Ge and t-Sn mixture was heated at 15.9 GPa, then melted, followed by temperature quenching and decompression to ambient pressure (Figure 1). As seen in Figures 1a, c, upon heating at 15.9 GPa, the diffraction patterns of both t-Sn and  $\beta$ -Ge decrease in intensity. Interdiffusion between the two elements begins at about 400 K. Indeed between 298 and 548 K the leftmost t-Sn peak shifts from 5.038 to 5.057 degrees unlike the case upon heating pure t-Sn where it shifts like all other t-Sn peaks to the left due to thermal expansion. Shift to the right here means diffusion of Ge into Sn. At 756 K, the diffraction patterns of the starting phase structures have almost disappeared and three distinct diffraction peaks emerge which are indexed to the bcc structure with *Im* $\bar{3}$ *m* symmetry<sup>[11]</sup> (Figure 1a). The values of parameter *a* adjacent to individual peaks in the figures were evaluated for each of these peaks by assuming that the peaks belong to the *Im* $\bar{3}$ *m* phase (see also section 6 supplementary information).<sup>[15]</sup> If the *a*'s evaluated do not substantially differ from each other ( $< \approx 0.015 \text{ \AA}$ ) and from the lattice parameter *a* evaluated from Le Bail whole pattern fitting, then this supports the cubic assignment and concomitant absence of significant anisotropy.<sup>[15]</sup> If the pattern is not cubic the parameters will likely differ significantly and cannot be fit to cubic using Le Bail.<sup>[15]</sup> Upon further heating, the diffraction pattern of *Im* $\bar{3}$ *m* strengthens while residual other sample peaks largely vanish. At 777 K whole pattern fitting

(Le Bail method) provides a lattice parameter of 3.481 Å for the new phase (Figure 1a, Figure S6).<sup>[15]</sup> At 828 K the new phase melts. The only diffraction peaks remaining at this temperature are the broad MgO peaks of the encapsulating octahedron (Figure 1a, c). Upon cooling, only the first two diffraction peaks re-emerge, as measured at 674 K and at 298 K. These could only nominally be indexed to a distorted *Im* $\bar{3}$ *m* symmetry because the lattice parameters calculated from each of these peaks, differ now by more than 0.06 Å (Figure 1b,c, Figure S7).<sup>[15]</sup> This is unlike the case before melting where virtually no anisotropy is present and unlike the experiments with no melting, where no anisotropy is observed at any stage based on the fitting of individual peaks, the Le Bail whole pattern fittings and space group *Im* $\bar{3}$ *m* assignments documented in section 6 in the supporting information.<sup>[15]</sup> Upon decompression in this experiment (Figure 1b), this distorted *Im* $\bar{3}$ *m* phase, whose diffraction peaks also exhibit significant intensity variations, is preserved down to 4.2 GPa (Figures S7–12).<sup>[15]</sup> However below 10 GPa, Sn diffuses out of the structure, as seen by the emergence of  $\beta$ -Sn below this pressure. On recovery, *I4*<sub>1</sub>/*amd* and nanocrystalline *Fd* $\bar{3}$ *m* Ge-Sn alloys are obtained (Figure S3).<sup>[16,17]</sup> A multi-anvil experiment with the same starting composition as above but without melting is shown in Figure 2. The pattern evolution is very similar to that of the previous experiment upon heating (Figure 2a,c, Figure S13).<sup>[15]</sup> However in contrast to the previous experiment, upon temperature quenching no notable anisotropy or diffraction intensity variation is observed in the quenched *Im* $\bar{3}$ *m* phase (Figure 2b, top two

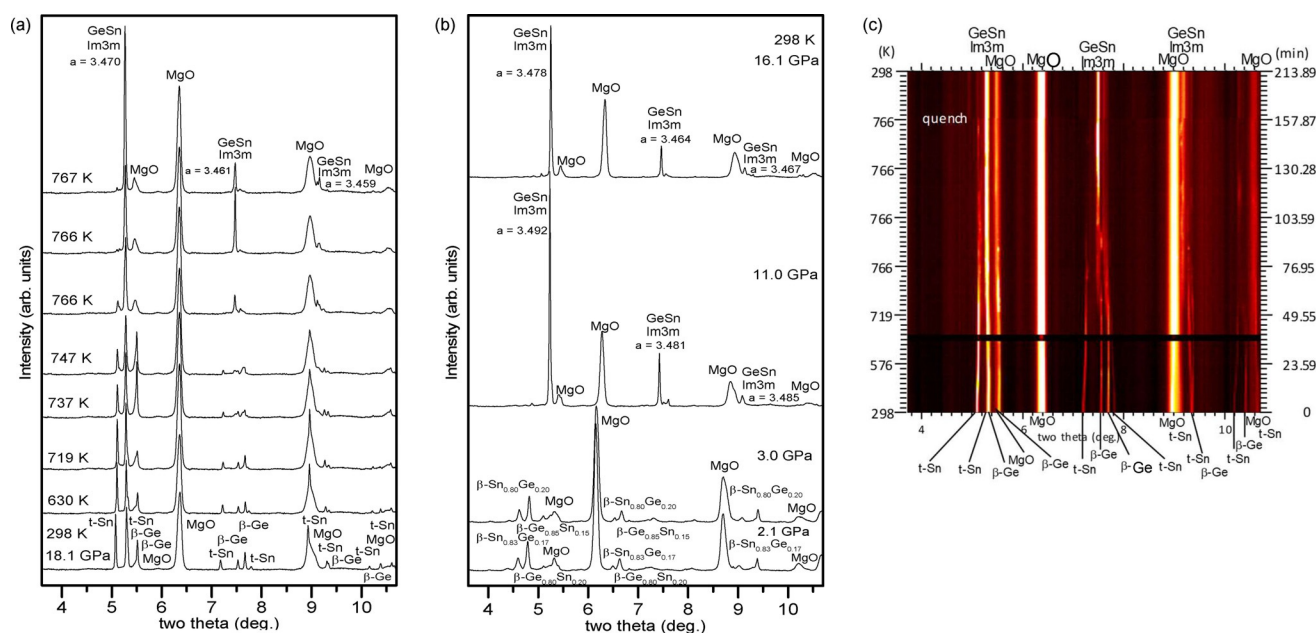


**Figure 2.** a) Angle-dispersive X-ray diffraction patterns upon heating of a  $\beta$ -Ge and t-Sn mixture at 18.1 GPa in a multi-anvil device and formation of a bcc structure with  $Im\bar{3}m$  symmetry ( $a = 3.457$  (1) Å) at 767 K (Figure S13, Le Bail fitting in the supporting information).<sup>[15]</sup> b) Decompression patterns still show the  $Im\bar{3}m$  symmetry at 11 GPa and  $\beta$ -Sn-rich and  $\beta$ -Ge-rich alloys at 3 and 2.1 GPa (Figures S14–17, Le Bail fitting in the supporting information).<sup>[15]</sup> c) Time-temperature-intensity-two-theta plot at 18.1 GPa in the solid state and upon temperature quenching. The left and right horizontal bars are not scales, but references to correlate times on the right vertical axis with their corresponding temperatures on the left vertical axis.

patterns, Figures S14,15). Below 10 GPa, Sn and Ge-rich alloys with  $I4_1/amd$  symmetry emerge (bottom two patterns, Figures S16,17). On recovery, Ge-Sn alloys with  $I4_1/amd$  and  $P4_32_1$  symmetries, as well as Ge with  $P6_3/mmc$  symmetry are obtained (Figure S4).<sup>[10,11,15–17]</sup>

We also present an example from our double-sided laser-heated diamond anvil cell experiments on synthesis of this new cubic alloy (Figure 3). A nominal 60:40 at%  $\beta$ -Ge and t-Sn mixture in a neon pressure medium was heated at 21 GPa.<sup>[18]</sup> As in the multi-anvil experiments described above, as the temperature was raised, the diffraction peaks associated with the endmember Ge and Sn phases weakened and largely vanished and were replaced by a diffraction pattern containing only the new  $Im\bar{3}m$  phase together with neon diffraction peaks (Figure 3a, Figure S18).<sup>[15]</sup> Upon decompression (Figure 3b) the new cubic phase is still observed at 11 GPa, whereas below 10 GPa the GeSn  $Im\bar{3}m$  phase disproportionates into Sn-rich and Ge-rich tetragonal phases with  $I4_1/amd$  symmetry (Figure S19–22).<sup>[15]</sup> On recovery in this experiment, pure Ge with  $Ia\bar{3}$  symmetry, Sn-rich  $I4_1/amd$  and Ge-rich  $Fd\bar{3}m$  were observed (Figure S5).<sup>[15,19,20]</sup> An example of a synthesized  $Im\bar{3}m$  phase from a nominal 60:40 at%  $\beta$ -Ge and t-Sn starting mixture, using an argon pressure medium,<sup>[21]</sup> at 21 GPa after quenching, is also shown in Figure 4 (Figure S23).<sup>[15]</sup>

## Discussion

With the unexpected formation of this new cubic phase established, we now consider the several unusual aspects

associated with this synthesis. The first is the atomic radii incompatibility of endmember Ge and Sn for solid solution formation. The endmembers  $\beta$ -Ge and t-Sn with their different crystal structures also have atomic radii which markedly differ from each other by about 18% throughout the 13 to 28 GPa synthesis regime.<sup>[15,16,22]</sup> Despite this incompatibility and operation well outside the apparent singular compatibility “sweet spot” of 10 GPa, cubic solid solutions with  $Im\bar{3}m$  symmetry were prepared throughout the 13–28 GPa regime (Figures 1–4).<sup>[15]</sup> The explanation for this, is that the atomic radii within the coordination polyhedra of the endmember structures are not the appropriate compatibility manometer here. It is instead, the radii that the elements will adopt in the coordination polyhedra of the new structure. Ge in  $\beta$ -Ge is coordinated to 4+2 nearest neighbours.<sup>[11]</sup> In the cubic structure with  $Im\bar{3}m$  symmetry however, Ge is coordinated to 8 nearest neighbours.<sup>[11]</sup> An expression introduced by Pauling<sup>[23]</sup> allows us to estimate a Ge radius in eightfold coordination resulting in a radius expansion of about 15% from that in sixfold coordination.<sup>[15]</sup> Sn only starts forming this cubic structure above 40 GPa and completely above 70 GPa,<sup>[24]</sup> but its radii in our lower pressure regime of synthesis can be evaluated through extrapolation from these higher pressures. With Ge and Sn both in 8-fold coordination, atomic radii ratios are estimated to be within 2% of each other, so well within the Hume-Rothery compatibility boundary of 15%<sup>[12,15]</sup> (Figure S2).

This however highlights the second unusual aspect of this synthesis.  $Im\bar{3}m$  Sn only exists as a single phase above 70 GPa. Our results show however, that incorporation of Ge in Sn lowers the formation pressure of a pure  $Im\bar{3}m$  phase by

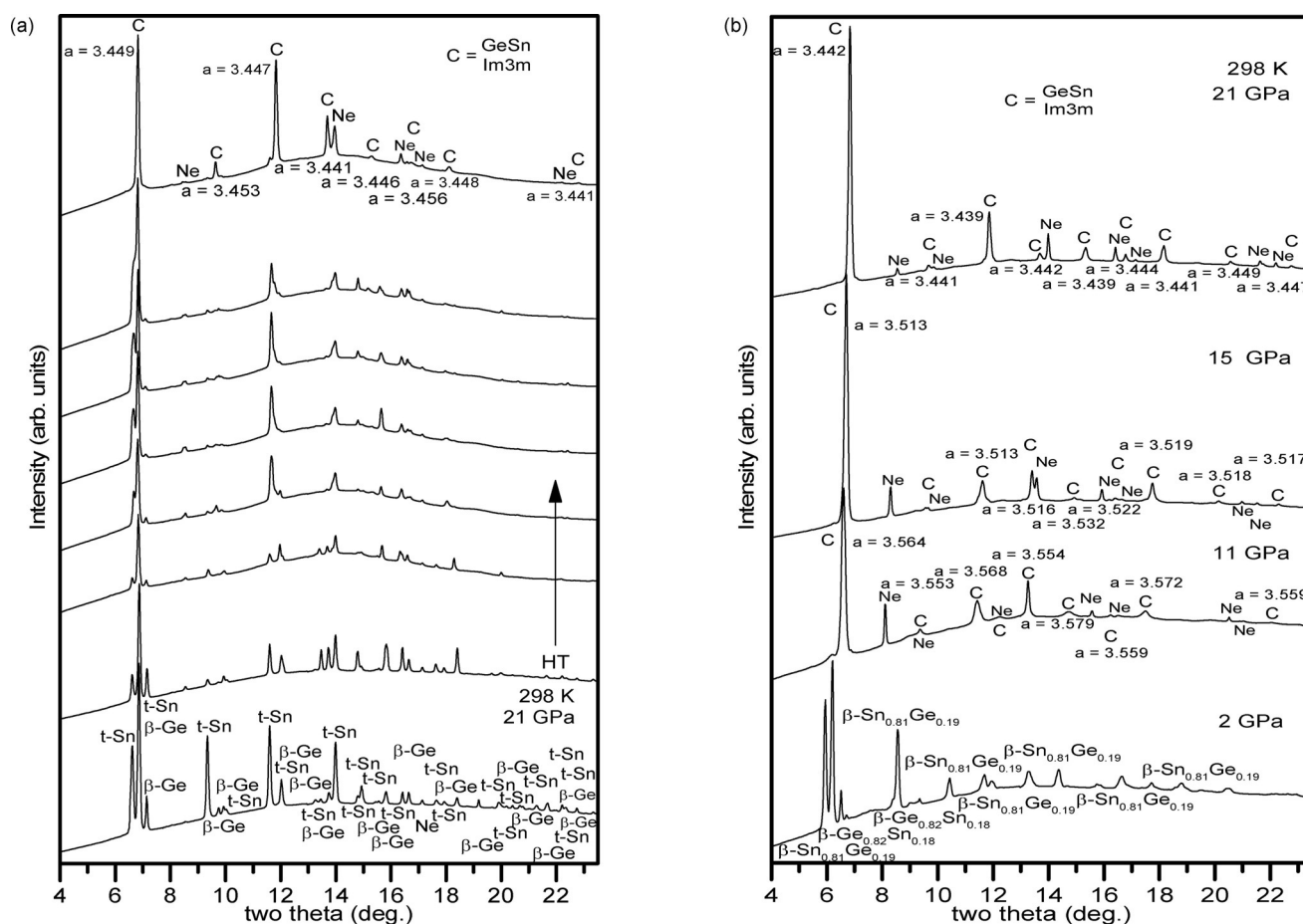


**Figure 3.** a) Angle-dispersive X-ray diffraction patterns upon heating of a  $\beta$ -Ge and t-Sn mixture at 21 GPa in a laser-heated diamond anvil cell and formation of a bcc structure with  $Im\bar{3}m$  symmetry  $\{a = 3.443(1) \text{ \AA}\}$  (top pattern) (Figure S18, Le Bail fitting in the supporting information)<sup>[15]</sup> in a neon pressure medium. b) Decompression patterns still show the  $Im\bar{3}m$  phase at 11 GPa and  $\beta$ -Sn-rich and  $\beta$ -Ge-rich alloys at 2 GPa (Figures S19–22, Le Bail fitting in the supporting information).<sup>[15]</sup>

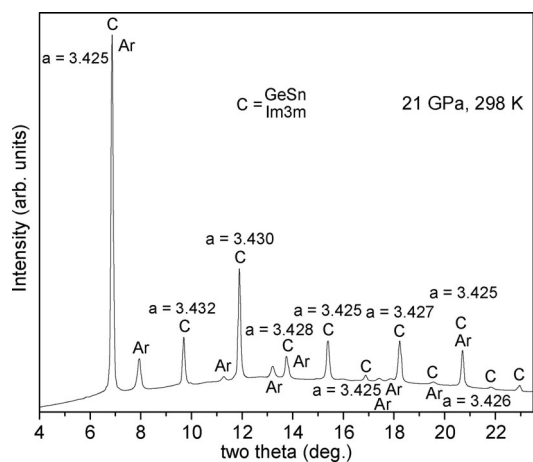


**Figure 4.** A bcc structure with  $Im\bar{3}m$  symmetry  $\{a = 3.429(1) \text{ \AA}\}$  (Figure S23, Le Bail fitting in the supporting information)<sup>[15]</sup> formed from a  $\beta$ -Ge and a t-Sn mixture at 21 GPa in a laser-heated diamond anvil cell in an argon pressure medium.

a striking 50 GPa. This dramatic lowering of  $Im\bar{3}m$  stabilization pressure cannot be attributed to chemical pressure alone

because the radius of Ge in the cubic structure with  $Im\bar{3}m$  symmetry is very similar to that of Sn. Ge promoting  $Im\bar{3}m$  formation is moreover, counter-intuitive because Ge, for very specific reasons presented below, does not form the  $Im\bar{3}m$  phase at any pressure. Therefore, Ge should hinder, not enhance formation of the  $Im\bar{3}m$  phase. In Ge namely, the s and p states are sufficiently close in energy that  $sp^3$  hybridization and the associated tetrahedrally coordinated diamond structure, are favoured.<sup>[25]</sup> With increasing pressure,  $sp^3$  hybridization only gradually becomes less favourable in Ge with respect to promotion of electrons from the s-state to the p-state. The ensuing higher pressure intermediate bonded and distant from cubic Ge structures with  $Im\bar{3}m$  symmetry are dictated by this s-p favourability interplay and the diamond structure.<sup>[11]</sup> This channeling away from the bcc ( $Im\bar{3}m$ ) structure for Ge (and Si) is terminated one row down in the group IVA column, with Sn, because in Sn, the s and p states are no longer very close in energy. Thus the s-p electron promotion cost does not exceed that gained from  $sp^3$  hybridization. Therefore the adoption upon compression of higher coordinated structures and the bcc symmetry in pure Sn are governed by the domination of de-hybridized p-electron states over sp hybridized ones.<sup>[11,25]</sup> However entropy can

have a significant stabilization effect on alloys,<sup>[26,27]</sup> and incorporation of Ge will contribute favourably in this regard. This stabilizing effect will be further strengthened with increasing temperature through  $T\Delta S$  in the Gibbs free energy expression. Hence we put forth, that in the solid solution of Sn with Ge, together with still prevalently occupied p-electron states due to Sn, an energetically dominant entropic contribution through Ge incorporation contributes to the profound lowering of the formation pressure of the bcc ( $Im\bar{3}m$ ) phase. Indeed, entropic stabilization of otherwise unstable systems has been demonstrated, in other binary systems.<sup>[26]</sup>

A third unusual aspect is that melting is disruptive to the synthesis. Conventionally, melting is integral to synthesis as a part of a standard protocol in facilitating homogenization and more efficient reaction between starting materials, resulting in higher quality reaction products. Here, however, the opposite is true. We documented namely that melting is detrimental to formation of the isotropic cubic structure ( $c/a = 1$ ) with  $Im\bar{3}m$  symmetry (Figure 1) even with post-melt annealing, or even in other experiments, to complete inability to temperature-quench the new cubic phase, even if it had fully formed before melting. In sharp contrast, solely sub-liquidus annealing, where phase formation is governed by solid state diffusion is vital for high quality  $Im\bar{3}m$  crystal development (Figures 1–4). An explanation for this is because the Sn liquid structure is considerably more anisotropic than the underlying Sn crystal structure, at the same pressure.<sup>[28,29]</sup> This is because a significant (50%), highly anisotropic  $\beta$ -Sn structural component ( $c/a = 0.54$ ), is present in the liquid state even at 20 GPa, whereas in the solid state,  $\beta$ -Sn  $I4_1/amd$  ( $c/a = 0.54$ ) completely transforms to t-Sn ( $c/a = 0.9$ ) at 10 GPa.<sup>[19,28]</sup> Hence on melting, templating to highly anisotropic local  $\beta$ -Sn units hinders quenching of the new ( $c/a = 1$ ) phase, in sharp contrast to interdiffusion upon heating in the solid state where the structural environment is considerably less anisotropic. Solid state reaction is also assisted by the low activation barrier for diffusion of Sn, where noticeable diffusion already starts as low as 391 K.<sup>[15]</sup> By employing solid state reaction exclusively, not only is the quality of the synthesized crystals much better, but the  $Im\bar{3}m$  alloy could be recovered to room temperature at lower pressures than when attempting to quench after melting, even with post-melt annealing.

A fourth unusual attribute of this synthesis is that the specific volumes of t-Sn,  $\beta$ -Ge and our new cubic  $Im\bar{3}m$  solid solution, indicate that not more than about 15 at % Ge should dissolve into Sn.<sup>[15]</sup> However the evolution of diffraction patterns in both the multi-anvil and the diamond anvil experiments reveal upon solid state heating, the emergence and strengthening of the  $Im\bar{3}m$  solid solution pattern with a gradual decline of the other sample patterns until the  $Im\bar{3}m$  solid solution pattern dominates (Figures 1–4). The explanation towards this is the marked influence that temperature has on the relative specific volumes of the reactants and products. For example, just below the melting temperature of Sn at a given pressure,  $Im\bar{3}m$  solution with up to 46 at % Ge becomes favourable.<sup>[15]</sup> However the 60:40 starting Ge:Sn mix employed would still require a temperature exceeding the melting temperatures of the two components for complete incorporation. Also at the temperatures employed in the

multi-anvil experiments, solution of up to about 24 at % Ge in Sn is favourable. Because Sn ex-solves on decompression, the compositions during decompression and upon recovery are not those of the new cubic phase, even though, they are often Ge-rich.

## Conclusion

These results are also a fountainhead for exploring and exploiting new materials landscapes that include semimetals, post-transition metals as well as semiconductors, for both technological and fundamental benefit.<sup>[30]</sup> Here, we are completing in situ experiments on a binary solid solution formed at 10 GPa, which serves as the structural and electronic bridge between the known cubic  $Fd\bar{3}m$  regime and the new cubic  $Im\bar{3}m$  regime. Together with its crystal chemical importance we will exploit this “sweet spot” solid solution using its known composition as a single phase synthetic vehicle, to pinpoint the composition of our cubic  $Im\bar{3}m$  solid solutions. We have also recovered a range of binary structures, including tetragonal  $P4_32_12$ , hexagonal  $P6_3mmc$ , cubic  $Ia\bar{3}$  and nanocrystalline cubic  $Fd\bar{3}m$  phases with optoelectronic potential, that we are currently investigating. Moreover, configurational entropy, plays an important role in stabilizing the cubic  $Im\bar{3}m$  solid solution. Hence we are also expanding the compositional range of the new cubic phase by introducing further components,<sup>[31]</sup> silicon in the first instance, which can also provide increased optoelectronic tunability. Additionally, we are using high pressure and temperature synthesis in conjunction with low temperature decompression as an additional avenue for stabilizing the new phase on recovery. The emergence of this previously hidden group IVA alloy structure is thus itself a source for further enrichment, of what is arguably the most technologically important column of the periodic table.

## Acknowledgements

Parts of this research were carried out at P02.2/PETRA at the German Electron Synchrotron (DESY), a member of the Helmholtz Association (HGF) in the context of DESY-D-I-20140753 and DESY-D-I-20160758. Parts of this research were also carried out at ID06 at the European Synchrotron Radiation Facility (ESRF) in the context of CH4897, CH5244 and CH5596. We gratefully thank both institutions for their support. We also thank Mike Hall, Owen McDowall, Luke Fulford, Patrick Mortimer, Reik Sunkel and Andreas Ebert for contributing to component micromanufacture, assembly and characterization as well as Laura Serghiou for assistance with manuscript processing and Laurence Nigay and Costas Serghiou for incisive comments on the manuscript.

## Conflict of interest

The authors declare no conflict of interest.

**Keywords:** alloys · angle dispersive X-ray diffraction · materials synthesis · pressure and temperature · solid solution

- 
- [1] M. S. Hybertsen, S. G. Louie, *Phys. Rev. B* **1986**, *34*, 5390–5413.
- [2] R. Braunstein, A. R. Moore, F. Herman, *Phys. Rev. B* **1958**, *109*, 695–710.
- [3] G. Serghiou, G. Ji, M. Koch-Müller, N. Odling, H. J. Reichmann, J. Wright, P. Johnson, *Inorg. Chem.* **2014**, *53*, 5656–5662.
- [4] S. Wirths, R. Geiger, N. von den Driesch, G. Mussler, T. Stoica, S. Mantl, Z. Ikonic, M. Luysberg, S. Chiussi, S. J. M. Hartmann, H. Sigg, J. Faist, D. Buca, D. D. Grutzmacher, *Nat. Photonics* **2015**, *9*, 88–92.
- [5] K. P. Homewood, M. A. Lourenco, *Nat. Photonics* **2015**, *9*, 78–79.
- [6] a) S. Biswas, J. Doherty, D. Saladukha, Q. Ramasse, D. Majumdar, M. Upmanyu, A. Singha, T. Ochalski, M. A. Morris, J. D. Holmes, *Nat. Commun.* **2016**, *7*, 11405; b) A. Elbaz, D. Buca, N. von der Driesch, K. Pantzas, G. Patriarche, N. Zerounian, E. Herth, X. Checoury, S. Sauvage, I. Sagnes, A. Foti, R. Ossikowski, J. M. Hartmann, F. Boeuf, Z. Ikonic, P. Boucaud, D. Grutzmancher, M. El Kurdi, *Nat. Photonics* **2020**, *14*, 375–382.
- [7] T. Eales, I. P. Marko, S. Schulz, E. O'Halloran, S. Ghetmiri, W. Du, Y. Y. Zhou, S. Q. Yu, J. Margetis, J. Tolle, E. P. O'Reilly, S. J. Sweeney, *Sci. Rep.* **2019**, *9*, 14077.
- [8] C. L. Senaratne, P. M. Wallace, J. D. Gallagher, P. E. Sims, J. Kouvetakis, J. Menendez, *J. Appl. Phys.* **2016**, *120*, 025701.
- [9] T. Massalski, *Binary Alloy Phase diagrams*, Vol. 2, 2<sup>nd</sup> ed. (Ed.: T. Massalski), ASM, Ohio, **1990**.
- [10] C. Guillaume, G. Serghiou, A. Thomson, J. P. Morniroli, D. J. Frost, N. Odling, M. Mezouar, *J. Am. Chem. Soc.* **2009**, *131*, 7550–7551.
- [11] H. Katzke, U. Bismayer, P. Toledano, *Phys. Rev. B* **2006**, *73*, 134105.
- [12] W. Hume-Rothery, R. E. Smallman, *The Structure of Metals and Alloys*, 5<sup>th</sup> ed., The Chaucer Press, London, **1969**.
- [13] G. Serghiou, C. L. Guillaume, C. E. Jeffree, A. Thomson, D. J. Frost, J. P. Morniroli, N. Odling, *High Pressure Res.* **2010**, *30*, 44–50.
- [14] C. L. Guillaume, G. Serghiou, A. Thomson, J. P. Morniroli, D. J. Frost, N. Odling, C. E. Jeffree, *Inorg. Chem.* **2010**, *49*, 8230–8236.
- [15] Supporting information.
- [16] A. Di Cicco, A. C. Frasini, M. Minicucci, E. Principi, J. P. Itie, P. Munsch, *Phys. Status Solidi B* **2003**, *240*, 19–28.
- [17] M. E. Cavaleri, T. G. Plymate, J. H. Stout, *J. Phys. Chem. Solids* **1988**, *49*, 945–956.
- [18] A. Dewaele, F. Datchi, P. Loubeyre, M. Mezouar, *Phys. Rev. B* **2008**, *77*, 094106.
- [19] A. Mujica, A. Rubio, A. Munoz, R. J. Needs, *Rev. Mod. Phys.* **2003**, *75*, 863–912.
- [20] H. Wang, J. F. Liu, Y. He, Y. Wang, W. Chen, J. Z. Jiang, J. Staun Olsen, *J. Phys. Condens. Matter* **2007**, *19*, 1–10.
- [21] D. Errandonea, R. Boehler, S. Japel, M. Mezouar, *Phys. Rev. B* **2006**, *73*, 092106.
- [22] T. G. Plymate, J. H. Stout, M. E. Cavaleri, *J. Phys. Chem. Solids* **1988**, *49*, 1339–1348.
- [23] L. Pauling, P. Pauling, *Acta Crystallogr.* **1956**, *9*, 127–130.
- [24] A. Salamat, R. Briggs, P. Bouvier, S. Petitgirard, A. Dewaele, M. E. Cutler, F. Cora, D. Daisenberger, G. Garbarino, P. F. McMillan, *Phys. Rev. B* **2013**, *88*, 104104.
- [25] N. E. Christensen, M. Methfessel, *Phys. Rev. B* **1993**, *48*, 5797–5807.
- [26] A. Manzoor, S. Pandey, D. Chakraborty, S. R. Phillpot, D. S. Aidhy, *npj Comput. Mater.* **2018**, *47*, 1–10.
- [27] N. Dragoe, D. Berardan, *Science* **2019**, *366*, 573–574.
- [28] T. Narushima, T. Hattori, T. Kinoshita, A. Hinzmann, K. Tsuji, *Phys. Rev. B* **2007**, *76*, 104204.
- [29] T. Weir, M. J. Lipp, S. Falabella, S. Samurdrala, Y. K. Vohra, *J. Appl. Phys.* **2012**, *111*, 123529.
- [30] a) E. M. T. Fadaly, A. Dijkstra, J. R. Suckert, D. Ziss, M. A. J. van Tilburgh, A. J. Marvin, C. Y. Mao, Y. Z. Ren, V. T. van Lange, K. Korzun, S. Kolling, M. A. Verheijen, D. Busse, C. Roedel, J. Furthmüller, F. Bechstedt, J. Stangl, J. J. Finley, S. Botti, J. E. M. Haverkort, E. P. A. M. Bakkers, *Nature* **2020**, *580*, 205–209; b) M. Kanatzidis, H. Sun, S. Dehnen, *Inorg. Chem.* **2020**, *59*, 3341–3343; c) A. Minelli, S. M. Souliou, T. Nguyen-Thanh, A. H. Romero, J. Serrano, W. Ibarra Hernandez, M. J. Verstraete, V. Dmitriev, A. Bosak, *Phys. Rev. B* **2019**, *100*, 104305.
- [31] D. A. Young, *Phase diagrams of the elements*, **1991**, University of California Press, Berkeley.

Manuscript received: December 4, 2020

Accepted manuscript online: February 2, 2021

Version of record online: March 9, 2021